TELLUS

On the origin of interdecadal oscillations in a coupled ocean–atmosphere model

By OLIVIER ARZEL[1]*, ALAIN COLIN DE VERDIÈRE[2] *and* THIERRY HUCK[2], [1]*Climate and Environmental Dynamics Laboratory, School of Mathematics and Statistics, University of New South Wales, NSW 2052, Sydney, Australia;* [2]*Laboratoire de Physique des Océans, Université de Bretagne Occidentale, 6 Avenue Le Gorgeu, C.S. 93837, 29238 Brest cedex 3, France*

ABSTRACT

Interdecadal oscillations are analysed in a coupled ocean–atmosphere model made of a planetary geostrophic ocean model within an idealized geometry, coupled to a zonally-averaged tropospheric atmosphere model. The interdecadal variability that arises spontaneously in this coupled system is caused by intrinsic ocean dynamics, the coupled air-sea feedbacks being not essential. The spatial pattern of the variability bears some resemblance with observations and results obtained with atmosphere-ocean general circulation models (AOGCMs) as well as simpler climate models: large and quasi-stationary upper ocean temperature-dominated density anomalies are found in the north-western part of the ocean basin along with weaker, westward propagating anomalies in the remaining interior. The basic physical mechanism that lies at the heart of the existence of the interdecadal mode is a large-scale baroclinic instability of the oceanic mean flow in the vicinity of the western boundary, characteristic of ocean models forced by constant surface fluxes. Freshwater feedbacks associated with the hydrological cycle are found to have only a modest influence on the interdecadal mode. The presence of a periodic channel mimicking the Antarctic Circumpolar Current at high southern latitudes prevents the oceanic baroclinic instability to occur in the Southern Hemisphere.

1. Introduction

A proper detection of anthropogenic climate change requires a clear understanding of internal climate variability on timescales at which human influence on climate is most likely to occur (Houghton et al., 2001). These timescales are precisely in the decadal to centennial range. Multiproxy-based climate reconstructions of global surface temperature variations over the past centuries have revealed a distinct oscillatory mode of variability with an approximate timescale of 50–100 yr (Schlesinger and Ramankutty, 1994; Mann et al., 1998; Delworth and Mann, 2000; Gray et al., 2004). These long timescales suggest that the ocean dynamics, and in particular the thermohaline circulation, may play an important role. In the Atlantic Ocean, the spatial pattern associated to these long timescales is characterized by surface temperature anomalies of opposite sign between the Northern and Southern Hemispheres (NHs and SHs), suggesting a potential influence of variations in ocean heat transport associated with the large-scale Atlantic meridional overturning circulation (AMOC) (Mann et al.,

1998). In addition, observational studies using instrumental records support the existence of decadal to multidecadal variability in the North Atlantic climate system (Deser and Blackmon, 1993; Kushnir, 1994; Hansen and Bezdek, 1996; Reverdin et al., 1997; Delworth and Mann, 2000; Hakkinen, 2000). The role of ocean dynamics in Atlantic interdecadal variability was then investigated using atmosphere–ocean general circulation models (AOGCMs) as well as simple climate models. Studies conducted with the second group of climate models have mostly focused on the response of the AMOC to simple boundary conditions at the ocean surface which do not represent changes in the hydrological cycle. The purpose of this paper is thus to go a step further by analysing the interdecadal climate variability in an idealized coupled ocean–atmosphere model including an interactive hydrological cycle.

Delworth et al. (1993) obtained irregular variations of the AMOC in the Geophysical Fluid Dynamics Laboratory (GFDL) coupled model with enhanced variance around the 50-yr timescale. Similarities with observations of sea surface temperature (SST) by Kushnir (1994) and sea surface salinity (SSS) by Levitus (1989) were found. The key ingredient of their multidecadal variability is based on the interaction between the thermohaline and gyre (non-zonal) circulations and the phase lag between changes in SSS and SST appears crucial. The influence

of the atmosphere remains unclear but does not seem to play a major role. This latter point was further examined by Weaver and Valcke (1998) who forced with fixed surface fluxes the same ocean model used by Delworth et al. (1993). These authors concluded that the multidecadal variability that arises in the fully coupled GFDL model is not an ocean-only phenomenon as suggested previously by Delworth et al. (1993), but is rather related to coupled processes. Later, Delworth and Greatbatch (2000) found that the multidecadal thermohaline circulation variability that emerges in an updated version of the GFDL coupled model is driven by the low-frequency variations of the surface heat flux generated internally within the atmospheric model. Within the Max-Plank-Institute climate model, Timmermann et al. (1998) found a coupled mode and emphasized the crucial role of mid-latitudes atmospheric response to SST anomalies in the coupled variability. More recently, Dong and Sutton (2005) found a 25-yr damped oscillation of the AMOC in the HadCM3 climate model whose mechanism appears similar to that obtained by Delworth et al. (1993) and Delworth and Greatbatch (2000), with the variability primarily forced by the atmosphere. Within the same model, Vellinga and Wu (2004) analysed the centennial scale Atlantic thermohaline circulation variability: they found a coupled mechanism involving displacements of the ITCZ, generating salinity anomalies that are slowly advected northwards and modify the overturning several decades later.

The climate evolution simulated by coupled AOGCMs may operate in different regimes and is generally difficult to interpret because of the multiple simulated processes. There is still no consensus on the mechanisms which lie at the heart of the existence of interdecadal variability of the AMOC as simulated by AOGCMs. An alternative approach is thus to use simple climate models that allow to determine in detail the physical mechanism underlying a particular phenomenon and to propose hypotheses that can further be tested in more complex climate models. This idealized approach is especially useful, and even necessary, to make progress in understanding long-term climate variability for which basin-wide wave propagations and large-scale climate feedbacks occur. The first idealized climate model to explore decadal variability was put forward by Saravanan et al. (2000). Mid-latitudes decadal variability was found in a two-hemisphere oceanic spherical sector coupled to a two level atmosphere and the oceanic response shown to be made of two parts, a passive oceanic red noise response to stochastic atmospheric forcing and an active mode of oceanic variability with a periodicity of 16–20 yr. Although coupled ocean–atmosphere interactions did not appear to play a significant role, the coupling was judged important in selecting the scales of the oceanic variability.

With such idealized configurations, the uncoupled oceanic response shows two types of interdecadal variability associated to two different surface boundary conditions for temperature and salinity: the flux boundary conditions (FBCs) with time-independent surface heat and freshwater fluxes and the mixed boundary conditions (MBCs) which consist in a restoring bound-

ary condition for SST and a constant freshwater flux. Using a flat-bottom coarse resolution ocean model forced with prescribed surface heat flux, Greatbatch and Zhang (1995) obtained regular oscillations with a period of 50 yr and pointed out similarities with the previous climate model results of Delworth et al. (1993). Under MBCs, decadal to interdecadal oscillations were found very early (Weaver and Sarachik, 1991a,b; Weaver et al., 1991). Although an advective mechanism was first proposed, Arzel et al. (2006), identified the interaction of the perturbed surface heat flux with the convective adjustment as the cause of the growth of the perturbations. The interdecadal thermohaline oscillations obtained under these two kinds of idealized boundary conditions have been found to be of a completely different nature (Arzel et al., 2006). The most striking differences that allow to distinguish between them are the variable (T/S) controlling the density changes, the vertical structure of perturbations and the term governing the growth of density variance. Under FBCs, the density anomalies are intensified above the main thermocline and temperature-dominated whereas under MBCs, they extend more deeply and are salinity dominated. In the region of growth of oscillations (i.e. the most unstable region is defined as the area where the growth of density variance is strongest), the temperature and salinity anomalies are positively correlated at all depths under FBCs and exhibit a significant vertical phase lag of about a quarter period with the lower levels lagging upper ones. Under MBCs, the temperature and salinity anomalies are only positively correlated in the upper levels (above 200 m) because of the effect of the anomalous convective adjustment, and the temperature anomalies experience a strong dipolar structure in the vertical direction. Finally, the advection term $\overline{u'\rho'} \cdot \nabla\overline{\rho}$ dominates the growth of density variance under FBCs where the 'eddy part' (prime) is defined as the departure from a time-averaged (overbar). This term was associated with the long-wave limit of baroclinic instability in the vicinity of the western boundary current region by Colin de Verdière and Huck (1999), later generalized by te Raa and Dijkstra (2002), to explain the interdecadal variability under FBCs. By contrast, the forcing term $\overline{\rho'B'}$, where B' represents the surface heat flux anomaly, dominates the growth of density variance under MBCs. The basic interpretation of this term led Arzel et al. (2006) to conclude that a necessary condition to trigger variability under MBCs is that the correlation between temperature and salinity anomalies in the mixed layer must be positive and larger than the perturbation density ratio, which is a measure of the thermal against haline dependence of density. Given an initial perturbation, the underlying physical mechanism responsible for the growth of oscillations under MBCs was identified as a positive feedback between the anomalous convective adjustment and the perturbed surface heat flux (Arzel et al., 2006). A more physically appealing surface boundary condition compared to either FBCs or MBCs is to use a diagnostic energy balance model (EBM). The interdecadal oscillations obtained in climate models using such a coupling were shown to be the same as the ones forced by fixed surface

fluxes (Chen and Ghil, 1996; Huck et al., 2001), even with the added presence of sea ice (Kravtsov and Ghil, 2004). However, the variability may be damped out for sufficiently low or large heat transfer coefficient with the atmosphere (Huck et al., 2001).

Under FBCs, increased horizontal mixing, wind stress forcing and bottom topography are damping influences (Winton, 1997; Huck et al., 1999, 2001) but the damping rates are small, so that additional stochastic forcing from either atmospheric or oceanic transients may be sufficient to sustain the oscillation as emphasized by Huck et al. (2001). Compared to FBCs, the variability under MBCs exists in a narrower window of relevant model parameters such as vertical mixing (Weaver et al., 1993) or heat bulk transfer coefficient (Arzel, 2004). In summary, idealized studies of ocean only models have revealed two types of interdecadal variability of the thermohaline overturning: a mixed-type variability (under MBCs), and a flux-type variability (under fixed or quasi-steady surface fluxes). It should be noted, however, that the flux-type variability can also appear under restoring or MBCs if the density anomalies are damped on timescales larger than the e-folding timescale of long-wave baroclinic instability. Huck et al. (2001) showed this to occur when the heat transfer coefficient with the atmosphere did not exceed a critical value of 25 W m^{-2} K^{-1}. By contrast, the mixed-type variability cannot occur under FBCs since a positive feedback between the anomalous surface heat flux and the convective adjustment is required. Note finally that the mixed type variability can also appear under restoring boundary conditions used for both temperature and salinity provided that the restoring timescale for salinity is large enough.

After showing its potential for ocean only models, the methodology developed in Colin de Verdière and Huck (1999) and Arzel et al. (2006) could be quite useful as well to infer further the origin of the interdecadal variability found in the coupled models studies of Delworth et al. (1993), Delworth and Greatbacth (2000), and Dong and Sutton (2005). Saravanan et al. (2000), found that the similarities in the EOF structures of the oceanic response in an idealized coupled model and in a forced oceanic case suggested a MBCs origin. Yet the localization of the variability in the northwest corner of their oceanic basin, and the importance of the perturbed flow advecting the mean temperature indicate to us a possible alternative FBCs origin. Henceforth a primary objective of the present paper is to show the potentials of the methodology developed previously for ocean models for attributing an origin to the decadal variability in an idealized coupled model.

It is worth noting that the flux- and mixed-type oscillations have been obtained using models neglecting variations in the hydrological cycle (Weaver and Sarachik, 1991a,b; Weaver et al., 1991; Chen and Ghil, 1995, 1996; Greatbatch and Zhang, 1995; Colin de Verdière and Huck, 1999; te Raa and Dijkstra, 2002, 2004; Kravtsov and Ghil, 2004). However, the hydrological cycle has a major influence on the thermohaline circulation. In the Atlantic Ocean, changes in its strength can disrupt the

overturning circulation by modifying the salinity in the sinking regionsof the North Atlantic. It is thus the second objective of this paper to examine the robustness of these modes to additional freshwater feedbacks associated to an interactive hydrological cycle. To do so, a simplified model has been built around an idealized geometry 3-D planetary geostrophic ocean coupled to a 2-D zonally averaged statistical-dynamical atmosphere. The atmospheric model is particularly simple because we exclude a priori the synoptic variability by using a zonally averaged representation which filters out unstable baroclinic waves. By doing so, the passive red noise oceanic response to the stochastic atmospheric forcing does not appear allowing for much simpler analyses.

The remainder of this paper proceeds as follows. The coupled model and its climatology are described in Sections 2 and 3 respectively. The simulated interdecadal variability and the physical mechanism responsible for its existence are analysed in Section 4. The influence of a southern channel mimicking the Antarctic Circumpolar Current on the variability is finally studied in Section 5 before conclusions are given in Section 6.

2. Model description

2.1. Oceanic component

We use a 3-D planetary geostrophic ocean model at coarse resolution in spherical coordinates to represent the AMOC, and its associated poleward heat transport. In this planetary geostrophic limit, the momentum equations become diagnostic and there is no production of mesoscale eddies. This kind of model is particularly well suited to the study of extra-tropical large-scale flows (Salmon, 1986; Colin de Verdière, 1988; Winton and Sarachik, 1993). The vertical mixing is fixed to 10^{-4} m^2 s^{-1} which is about an order of magnitude larger than in situ measurements carried out away from topography (Ledwell et al., 1993) but agrees with values inferred from the large-scale abyssal stratification (Munk, 1966). Munk and Wunsch (1998) stressed that a vertical mixing of about 10^{-4} m^2 s^{-1} is still needed in small regions of buoyancy flux from which the water masses are exported into the ocean exterior. Our vertical mixing is thus assumed to represent the large-scale diapycnal diffusivity. The horizontal diffusivity is fixed to 1000 m^2 s^{-1}, in the range of values deduced from floats trajectories in the North Atlantic (see, e.g. Ollitrault and Colin de Verdière, 2002). The domain is a flat-bottom sector of a sphere, with dimensions appropriate for the North Atlantic (64° in longitude, from 77°S to 77°N). The horizontal Laplacian viscosity is fixed to 10^5 m^2 s^{-1}. Note that a two-hemisphere ocean model rather than two mirrored single hemispheric basins has been chosen in order to be consistent with the seasonal solar forcing applied to the top of the atmosphere and the associated cross-equatorial displacement of the ITCZ. Lateral boundaries are solid vertical walls where no-slip and no-FBCs are applied.

The model is run at a coarse horizontal resolution of about $2°$, with vertical grid spacing increasing from 50 m at the surface to 550 m at the bottom (15 levels, 4500 m deep). Finally, a linear equation of state is used in order to easily separate the influence of temperature and salinity on the variability.

2.2. Atmospheric component

In order to explore the nature and robustness of ocean generated interdecadal variability, the ocean model must be coupled to an atmospheric model with an active hydrological cycle. Because the coupled model has to be integrated for hundreds of years, a zonally averaged climate model (ZACM) was chosen for this purpose. Development of ZACMs flourished in the seventies (see the exhaustive review by McCracken and Ghan (1988)) but the constant improvement in computer power has opened the way to full blown atmospheric three dimensional models which are used routinely nowadays. We believe that the study of coupled ocean–atmosphere problems over secular and longer periods is one area where the ZACM remains an interesting choice with a complexity intermediate between that of a 3-D GCM and 1-D EBM. Besides the economy in calculation, the ZACM models also offer an economy in the analysis and sensitivity studies of their solutions which may be turned to an advantage.

One of their main difficulties concerns the parametrization of the meridional eddy transport of zonal momentum, heat and moisture. Pioneering works by Green (1970) and Stone (1972) have opened the road to such parametrizations which have been brought to an impressive degree of realism in a series of papers by Yao and Stone (1987), Stone and Yao (1987, 1990) and Genthon et al. (1990). This was made possible through the work of Branscome (1983) who computed the eddy fluxes due to the developing unstable baroclinic waves of the Charney problem. Our parametrization of eddy heat flux follows Stone and Yao (1990) while the eddy moisture fluxes parametrization is a simple diffusive closure since these fluxes are almost down the mean moisture gradient at least in the troposphere (Stone and Yao, 1990).

Finally the eddy momentum flux divergence is obtained after Green (1970). The parametrization conserves the global conservation of angular momentum as in Vallis (1982). To keep the atmospheric model as simple as possible, the grey atmosphere radiation scheme of Saravanan and McWilliams (1995) was used. A further difficulty concerns the representation of cumulus convection which occurs at scales two orders of magnitudes smaller than the synoptic scale. The moist convective adjustment of Manabe et al. (1965) was chosen and provided by L. Li (personal communication). To reduce the intensity of the high frequency instabilities that appears in the model ITCZ, the adjustment was calculated approximately every 6 hours and applied to both temperature and specific humidity with a restoring timescale of about 3 d (J. I. Yano, 2006, personal communication). In order to carry out long-term integrations, the full primitive equations were dis-
cretized on a staggered grid to conserve mass, momentum and energy. Further details of the atmospheric model are given in Table 1.

A simple land is parametrized polewards of the ocean boundary. We assume that the land is dry (no evaporation) and that the precipitation on land cannot accumulate and is then discharged instantaneously and uniformly as run-off along polar boundaries of the ocean basin. The land surface temperature, required by the atmospheric model, is simply determined by continuity using the zonally averaged meridional derivative of SST. For simplicity, we assume that, east and west of the ocean basin, the air–land heat and freshwater fluxes are identical to those over the ocean. This means that the zonally averaged atmosphere is forced with aqua-planet boundary conditions.

2.3. Coupling and sequence integration

The initial conditions are those of a homogeneous ocean and a dry isothermal atmosphere. The atmospheric model is first integrated for 2 yr with a prescribed zonally averaged SST varying seasonally that lags the seasonal solar forcing at the top of the atmosphere by about two months in order to crudely represent the effect of the oceanic mixed layer. The annual mean of the surface freshwater flux and wind stress over the last year of this atmospheric integration is then diagnosed and further applied to the ocean model, while the SST is restored towards the same restoring SST profile used in the atmosphere-only integration. Under these so-called MBCs, the ocean model is integrated until a steady state has been reached, after which it is coupled to the atmospheric model. This initialization procedure guarantees that the atmosphere and ocean are in quasi-equilibrium with each other at the beginning of the coupled integration since the surface fluxes are continuous. However, this matching is only approximate for the heat fluxes and the discrepancy is minimized by tuning the heat exchange coefficient to a value of $8 \text{ W m}^{-2} \text{ K}^{-1}$ in the ocean-only integration corresponding to a restoring timescale for SST of about 230 d for an uppermost level thickness of 50 m.

3. Time–mean states of the control experiment

We describe herein the annual mean climatology of the control experiment (CTRL, Table 2) which is based on a geometry symmetric with respect to the equator. The model climatology is defined as the average over several oscillation periods between years 300 and 400 of the coupled integration. We do not expect that the model climatology compares directly with observations because of the highly idealized model geometry employed but we rather do expect that the gross features of the observed present-day climate be reproduced.

3.1. Ocean mean state

The meridional overturning streamfunction features a two-cell structure symmetric with respect to the equator (Fig. 1). The

Table 1. Atmospheric model features

Geometry	Sphere $[-90, 90]$
Meridional discretization	Equal area increment: $dy = a\cos\Theta$ where Θ is latitude and a the earth radius
Vertical discretization	Equal increment in $\sigma = -\mathrm{H}\ln(p/p_0)$, with $H = 8.8$ km and $p_0 = 10^5$ N m^{-2}
Number of points in the meridional direction	$N_y = 80$
Number of points in the vertical direction	$N_\sigma = 20$
Meridonal eddy fluxes	Yao and Stone (1987)
Surface fluxes	Bulk formulae with a constant turbulent wind speed $u_{tu} = 5$ m s^{-1}
Sensible heat	$\rho_s\, c_h u_{tu}(t - sst)$ and $c_h = 1.3 \times 10^{-3}$
Evaporation	$\rho_s\, c_e u_{tu}(q - q_{sat}(sst))$ and $c_e = 1.3 \times 10^{-3}$
Wind Stress	$\rho_s C_D u_{tu}\mathbf{u_s}$ with $\mathbf{u_s}$ the surface wind velocity
Ground albedo	Two formulations: fixed and variable with temperature as in Saravanan and McWilliams (1995)
Infrared radiative fluxes	Grey atmosphere parameterization (wavelength independent emissivity), Saravanan and McWilliams (1995)
Cumulus convection	Manabe et al. (1965), routines from L. Li (LMD)
Vertical eddy viscosity	$a_v = 1$ m^2 s^{-1}
Vertical eddy diffusivity	$k_v = 1$ m^2 s^{-1}
Stencil of staggered grid	$\Psi\ w\ \Psi\ w$ $v\ T\ v\ T$ $\Psi\ w\ \Psi\ w$ Boundary conditions are imposed on v (w) points along vertical (horizontal) boundaries. Ψ is streamfunction.

strength of this circulation peaks at 24 Sv in each hemisphere with deep convection mainly occurring in a narrow latitude band poleward of 72° latitude and along the eastern boundary between 55° and 60° latitude. The wind-driven circulation (Fig. 2b) consists of three ocean gyres in each hemisphere, a tropical cyclonic cell (10 Sv), a subtropical anticyclonic cell (20 Sv) and a subpolar cyclonic cell (16 Sv). The annual mean SST (Fig. 3a) is characterized by a relatively zonal structure except close to the western boundary region where the meridional advection is the strongest (Fig. 3c). The SST decreases from 30°C at the equator to 4°C at both poleward ends. Similarly, the annual mean SSS (Fig. 3b) is quite zonal with a clear minimum (33 psu) at low latitudes, a tropical maximum extending westward from the eastern boundary, and a decrease further polewards. Elsewhere the interaction with the zonally averaged atmosphere makes the forcing rather independent of longitude and hence the SST and SSS response. Despite the stronger than observed meridional overturning, the oceanic poleward heat transport (not shown) peaks at only 0.6 PW at 35° latitude and is thus weaker than observational estimates of Trenberth et al. (2001) which rather give

a maximum of about 1 PW in the North Atlantic. This model deficiency could be attributed to the unrealistically symmetric structure of the meridional overturning that does not represent the northward heat transport at the equator.

3.2. Atmospheric mean state

The atmospheric model reproduces in a satisfying manner a tropical Hadley cell extending until 30° latitude with a maximum mass transport of about 10×10^{10} kg s^{-1}, and a Ferrel cell whose strength peaks at 2×10^{10} kg s^{-1} at mid-latitudes (Fig. 1). However, the model fails to simulate the observed weak polar cells found in the observations (Peixoto and Oort, 1992). At mid-latitudes, the annual mean atmospheric circulation is characterized by westerly jets (Fig. 4a) and enhanced meridional eddy momentum fluxes (not shown). The annual mean moisture (Fig. 4b) and in situ temperature distributions (Fig. 4c) display realistic values from low to mid-latitudes but appear too large in high latitudes, probably because of the too low planetary albedo there due to the absence of sea ice in our model. The annual

Table 2. List of experiments

CTRL	Control experiment of the fully coupled ocean-atmosphere model.
FLUX	Stand-alone ocean experiment. The atmospheric surface heat, freshwater and momentum flux averaged over one oscillation period of CTRL are diagnosed and further applied to the ocean model.
SHF_CST	Same as CTRL, but the surface heat flux applied to the ocean component is constant and equals that averaged over one oscillation period of CTRL.
FWF_CST	Same as CTRL, but the surface freshwater flux applied to the ocean component is constant and equals that averaged over one oscillation period of CTRL.
WIND_CST	Same as CTRL, but the surface wind-stress applied to the ocean component is constant and equals that averaged over one oscillation period of CTRL.
ACC	Periodic boundary conditions are applied to the ocean model between 77°S and 60°S from the bottom to the surface (no sill). The horizontal laplacian viscosity is increased compared to CTRL in order to simulate a magnitude of the zonal volume flux in the periodic channel that agrees with observations-based estimates.

mean downward surface heat and freshwater fluxes (Fig. 5) are fairly realistic, both in their spatial pattern and magnitude. Finally, the low bias in the equator-pole temperature contrast yields reduced mid-latitude eddy fluxes of sensible and latent heat that makes the poleward energy transport by the atmosphere too weak (2 PW) compared to observations (4 PW).

4. The interdecadal variability

In this section, we describe the model variability and determine the instability process that lie at the heart of the existence of the variability of the coupled system. Sensitivity experiments are further designed to assess the influence of surface forcings on the variability. We focus our analysis on the oceanic variability as it is anticipated that on interdecadal timescales the thermohaline overturning is likely to play an essential role. All the fields presented in this section are expanded over the NH as the variability is symmetric with respect to the equator. We choose the period between years 300 and 360 of the coupled integration as the reference period for the analysis of the oscillation.

4.1. Description of the variability

The coupled model generates a spontaneous interdecadal mode of variability with a period of 20 yr that is damped over a timescale of about 1000 yr (Fig. 6a). During the reference period, the maximum strength of the thermohaline overturning fluctuates around a mean value of 25 Sv with an annual mean peak to peak amplitude of about 5 Sv. Changes in wind-driven circulation remain weak, about 0.5 Sv for the annual mean standard deviation of the maximum strength of the subtropical and subpolar gyres. The spatial pattern of the variability is characterized by large-scale quasi-stationary surface-intensified density anomalies in northestern and southwestern corners of the two-hemisphere ocean basin (Fig. 7). In the ocean interior, weaker anomalies propagate westwards at depth against the mean eastward current at mid-latitudes (Fig. 8), and no clear westward propagation could be found either at the surface or at high latitudes at all
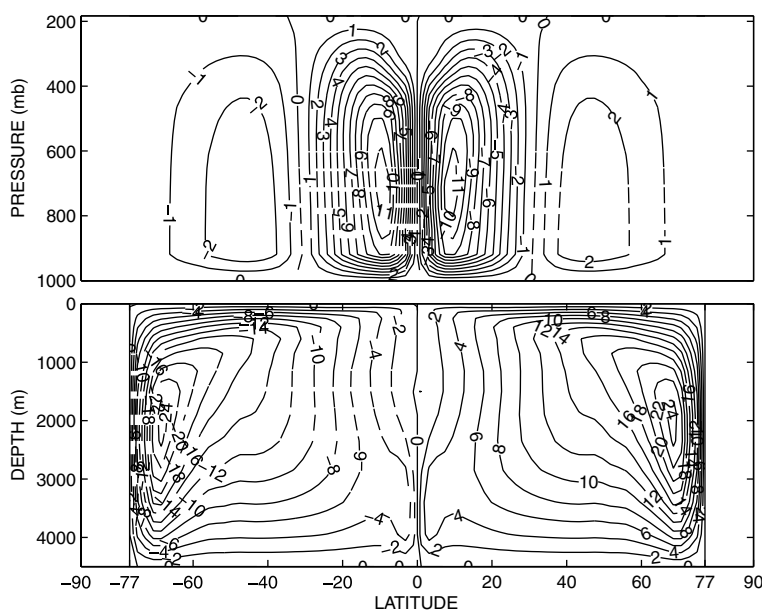

Fig. 1. Model climatology of the control experiment (CTRL). Zonally-averaged circulation in the atmosphere (top panel, megaton s^{-1}) and in the ocean (bottom panel, Sv, 1 Sv = 10^6 m^3 s^{-1}). The flow is clockwise around solid contours.
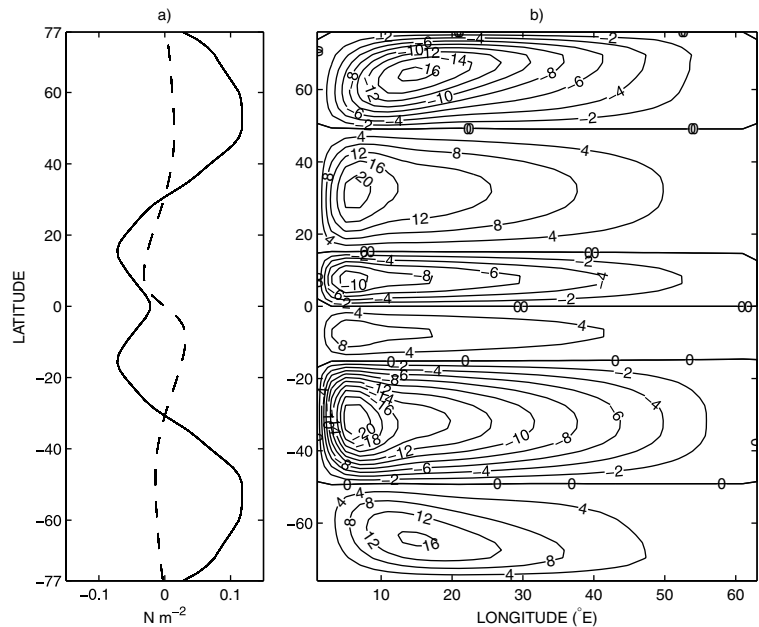
Fig. 2. Model climatology of the control experiment: (a) zonal (solid) and meridional (dashed) surface wind-stress; (b) corresponding barotropic streamfunction in the ocean (Sv). The flow is clockwise around solid contours.
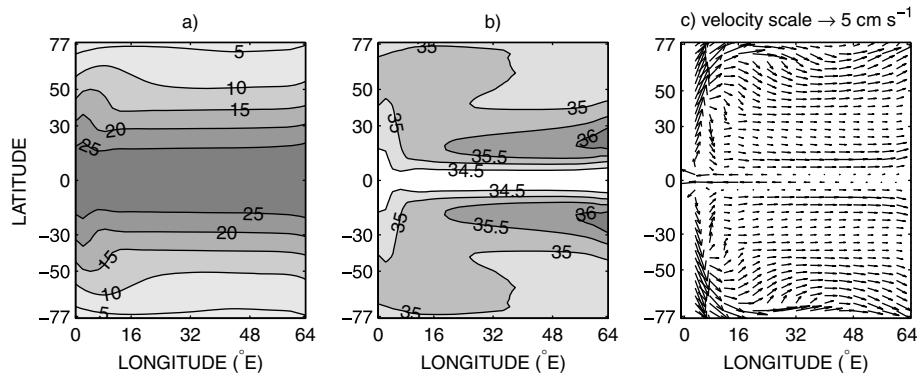

Fig. 3. Model climatology of the control experiment (CTRL): SST (a, °C), SSS (b, psu), and surface currents (c, arrows are shown every two grid points for better clarity).

depths. At low latitudes, density changes are weak and salinity dominated by contrast to mid to high latitudes where the temperature influence is the largest. Finally, the phase lag relationships between the zonal and meridional overturning and the meridional and zonal basin-wide temperature differences in the upper layers are similar (not shown) to those obtained by Huck et al. (1999), te Raa and Dijkstra (2002) and Kravtsov and Ghil (2004). Overall, the features that characterize the spatio-temporal pattern of the oceanic variability bear resemblance with the interdecadal mode obtained in purely ocean models forced by fixed surface heat flux and no salinity (Colin de Verdière et al., 1999; Huck et al., 1999; te Raa and Dijkstra, 2002; 2004). However, the magnitude of mid-latitudes perturbations at the surface in the ocean interior is somewhat weaker than in purely oceanic cases. These similarities suggest that we may witness a flux-type instability. This idea is further supported by the fact that the interdecadal variations in surface fluxes (heat, freshwater and momentum)

are small, indicating that the ocean–atmosphere feedbacks remain weak during the oscillation. The largest surface buoyancy flux changes appear in the western quadrant at high latitudes and represent only 6% of the mean surface forcing in this area. The wind-stress changes are dominant in mid-latitudes, between 45° and 70°N and do not exceed 4% of the mean surface wind stress.

4.2. The instability mechanism

To further elucidate the origin of the oceanic variability, we follow Colin de Verdière and Huck (1999) and Arzel et al. (2006) who provided various signatures of the interdecadal variability that emerges under FBCs and MBCs in the aim to differentiate them in more complex climate models, such as the one used in the present study. In particular, we determine first the term enabling the growth of density variance against all other damping sources, and second the vertical structure of density perturbations in this
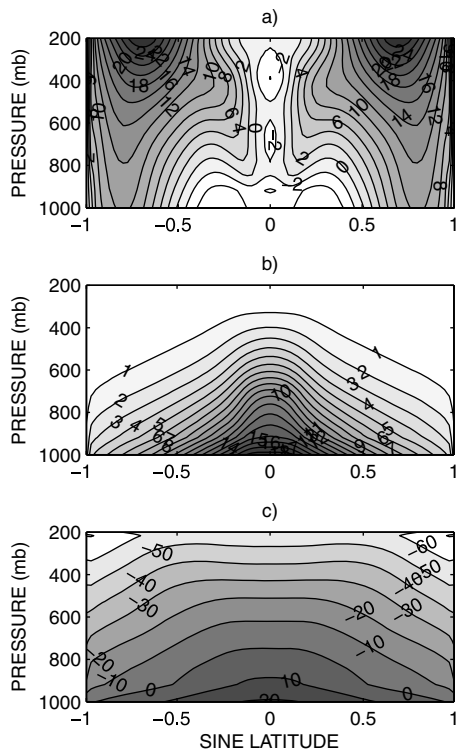
Fig. 4. Model climatology of the control experiment (CTRL): (a) zonal wind (m s^{-1}); (b) moisture (g kg^{-1}); (c) in-situ temperature (°C).

Fig. 5. Model climatology of the control experiment (CTRL): (a) total downward surface heat flux (turbulent + radiative, W m^{-2}); (b) freshwater flux (precipitation minus evaporation, cm yr^{-1}). Negative values are shaded. Note that only the turbulent fluxes (sensible, latent, evaporation) are non-zonal in the model, the radiative forcing as well as the precipitation remain zonal.

region of growth of the oscillations. Using the no-slip boundary conditions, the density variance budget averaged over the domain of interest and over time reads

$$\frac{1}{2}\left\langle \frac{\partial \overline{\rho'^2}}{\partial t} \right\rangle = -\langle \overline{u'\rho'}.\nabla\overline{\rho}\rangle + \langle H(z)\overline{\rho'B'}\rangle + \langle \overline{\rho'D'}\rangle, \qquad (1)$$

where the angle brackets denote a basin-wide average, and the prime the difference from the time average represented by the overbar, ρ is the density, u the 3-D velocity field and $H(z)$ the Heaviside step function that equals one in the forcing layer and zero elsewhere. The last term on the right-hand side of 1 is always negative and represents the diffusive sink of density variance, where D' combines the sum of all sub-grid scale diffusive (horizontal and vertical) and convective operators. Only the first two terms of the right-hand side can be positive and then generate variability. The first is indeed positive if the eddy fluxes are oriented down the mean density gradient. This term is familiar from baroclinic instability theory when the horizontal part of the density fluxes dominates and allow the transfer of potential energy from mean to unstable perturbations. This term has been pinpointed as the source of the variability in the constant flux experiments of Colin de Verdière and Huck (1999), for which the second term associated with the surface buoyancy flux B' vanishes.
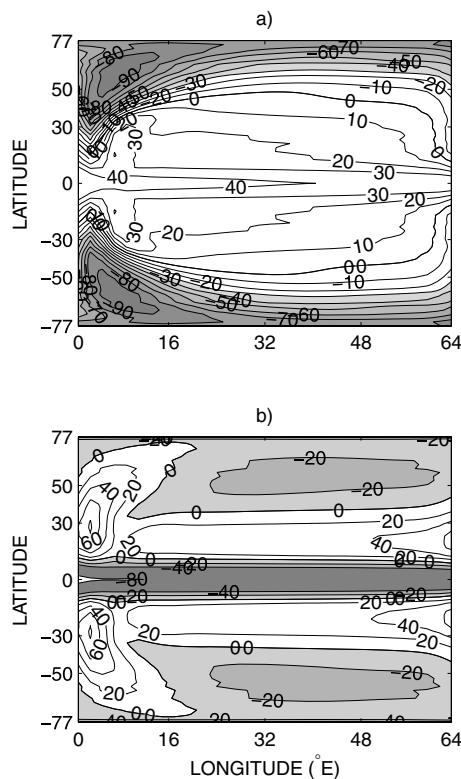
According to the results given in Table 3, the growth of density variance is clearly caused by the interaction of downgradient eddy temperature fluxes with the mean temperature gradient ($-\alpha^2\langle \overline{u'T'}.\nabla\overline{T}\rangle$). The contribution of salinity is negligible. The spatial pattern of this term averaged over one oscillation period shows large positive values in the northwest corner of each hemisphere and along the western boundary (Fig. 9). This region appears, therefore, as the source of energy for the oscillation. At high latitudes of the ocean interior, the negative values result in a local damping of the oscillation. Besides, the density perturbations in the region of growth of oscillations are characterized by a significant vertical phase lag between the surface and the lower levels that lag the upper anomalies by about one quarter of a period (Fig. 10). Note that no similar vertical phase lag has been found in the stable or neutral regions of the ocean interior. This specific vertical lag occurs in the baroclinic instability theory of a zonal mean flow and is the signature of heat transport by the unstable waves. The spatial pattern of the driving term in the density variance budget as well as the vertical structure of perturbations in the unstable region are similar to those found in ocean only models forced by constant surface fluxes (Colin
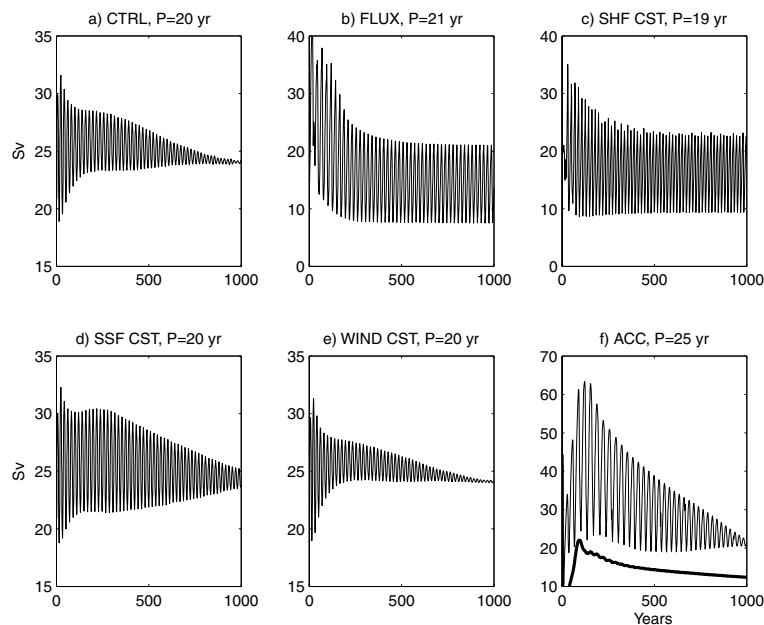
Fig. 6. Timeseries of the maximum meridional overturning streamfunction (Sv) in the Northern Hemisphere in (a) CTRL, (b) SSF_CST, (c) WIND_CST, (d) SHF_CST, (e) FLUX, (f) ACC. In f) the thick line indicates the maximum meridional overturning circulation in the Southern Hemisphere (values are multiplied by −1). Details of these experiments are given in Table 2. Note that the y-scale is different between (a, d, e), (b, c) and f. The period P of the variability is given for each experiment.

de Verdière and Huck, 1999; Arzel et al., 2006). We conclude, therefore, from these observations that the basic mechanism that lies at heart of the existence of the variability in our coupled model is a regional baroclinic instability of the mean flow in the vicinity of the western boundary region, characteristic of the behaviour of idealized ocean models forced by fixed surface fluxes. As emphasized by Colin de Verdière and Huck (1999), to equilibrate large heat losses at the surface in this region (Fig. 5a) by horizontal advection of heat requires large vertical shears that promote the baroclinic instability mechanism. Due to this instability, any imbalance caused for instance by inaccurate ocean adjustment to surface conditions at the beginning of the coupled integration will amplify rapidly.

We thus deduce from the *flux-type* nature of the oscillation that the interdecadal variability is not ascribed to coupled air–sea feedbacks, but rather to internal ocean dynamics and this is the central result of this paper. This result is confirmed by the stand-alone ocean experiment named FLUX which proceeds as follows. The surface buoyancy (Fig. 5) and momentum (Fig. 2a) fluxes over one oscillation cycle of the coupled integration are time averaged and applied to the ocean model for a further integration of about 1000 yr initialized from the mean state of CTRL. As expected, the decadal oscillation persists in this experiment (Fig. 6b) demonstrating that the air–sea feedbacks are not essential for its existence. This comparison shows further that the interdecadal variability obtained in ocean models forced by fixed surface fluxes is robust to additional freshwater feedbacks associated with the presence of an active hydrological cycle. This persistence of the oscillation in FLUX when there is no variability in the surface fluxes contrasts with Delworth and Greatbatch (2000) who found that the THC variations in the GFDL coupled

model can be viewed as an oceanic response to low-frequency fluctuations in surface heat flux forcing generated internally in the atmosphere model. Indeed, the self-sustained oscillations in FLUX demonstrates that the long-term damping of the variability observed in CTRL is caused by air–sea interactions rather than by intrinsic ocean dynamics (the amplitude of the oscillations has increased in FLUX compared to CTRL). This result can indeed be inferred from the density variance tendencies associated to the surface buoyancy forcing in Table 3. The corresponding negative values indicate that the freshwater flux, and more especially the surface heat flux have a damping influence on the growth of density variance. This thermal damping is mainly accomplished through the anomalous latent and sensible heat fluxes which both tend to decrease the growth rate of SST anomalies, the radiative forcing having a negligible but positive influence on the oscillations growth. The period of the variability in FLUX remains similar to that obtained in CTRL indicating that the adjustment of the oscillation cycle is again set by ocean dynamics rather than through air–sea interactions. The period was shown to be controlled by the westward propagation of mid-latitudes density anomalies (Fig. 8) against the mean eastward surface zonal flow (Colin de Verdière and Huck, 1999; te Raa and Dijkstra, 2002).

To summarize, the damping nature of the interactions with the atmosphere highlighted through both the density variance budget and the FLUX experiment demonstrates that the interdecadal variability of the coupled model is not caused by a mixed-type instability for which the interaction between changes in surface heat flux and anomalous convective motions are crucial (Arzel et al., 2006). This is in agreement with Delworth and Greatbatch (2000) who found that the variability in the GFDL coupled model differs from one forced by MBCs (Weaver and Sarachik, 1991).
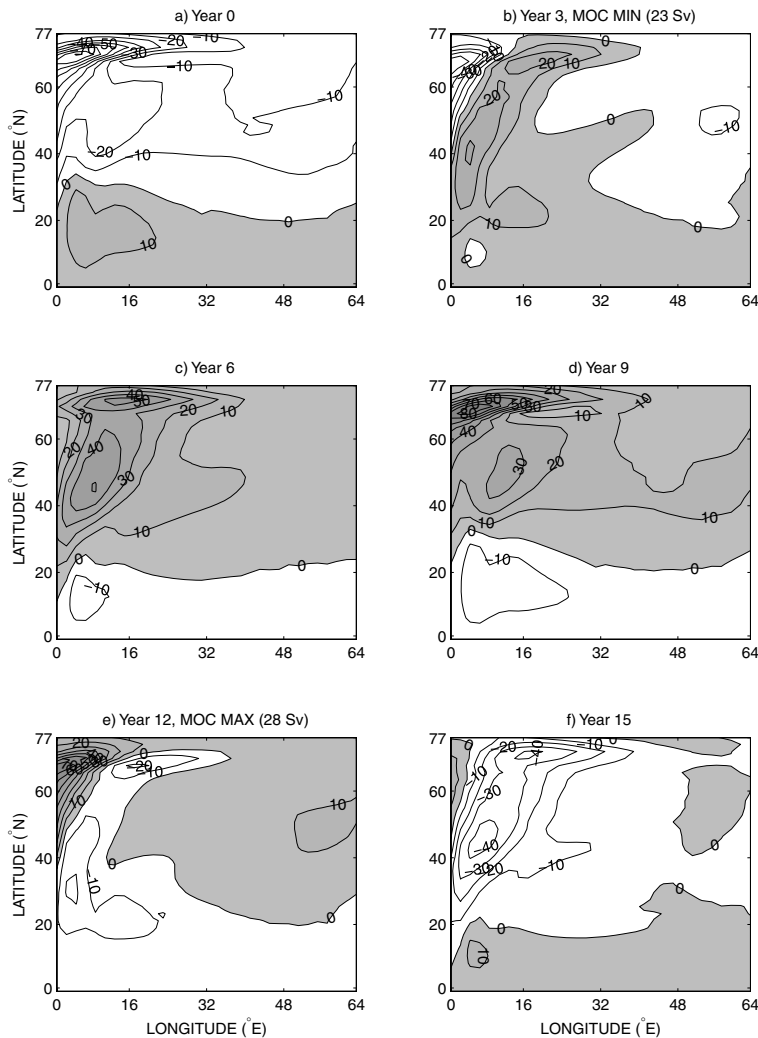
Fig. 7. Annual mean surface density anomalies ($\times 10^{-3}$ kg m^{-3}) during an oscillation cycle of CTRL. Positive values are shaded. Maximum an minimum meridional overturning circulation are indicated. The fields are expanded over the Northern Hemisphere as the variability is symmetric with respect to the equator.

4.3. Role of surface forcings in the variability

This FLUX experiment does not allow by itself to assess which surface forcings affect the variability. Additional sensitivity experiments summarized in Table 2 have been carried out to address this question. These are hybrid coupled ocean–atmosphere runs with an imposed surface forcing that can be either of heat, freshwater or wind stress. The results are visualized through the time-series of the overturning transport index shown in Fig. 6.

In the first experiment SHF_CST (Fig. 6c), the coupled model is run with the surface heat flux averaged over one oscillation period of CTRL. The stronger oscillations of this experiment demonstrate that the surface heat flux variability in the coupled model has a long-term damping influence on the variability in CTRL. In experiment SSF_CST (Fig. 6d), the coupled model uses the surface freshwater forcing averaged over one oscillation period of CTRL. The variability found in this experiment is very similar to that simulated in CTRL indicating that the changes in the hydrological cycle have no significant influence

on the variability. In experiment WIND_CST (Fig. 6e), the coupled model is run with the wind-stress forcing averaged over one oscillation period of CTRL and there is no significant difference with the time-series of the CTRL overturning index indicating that the wind-stress forcing variability has a modest influence on the thermohaline oscillation. Indeed, the impact of changes in surface wind stress during the oscillation is restricted to the upper layers and, therefore, affects weakly the deep thermohaline overturning responsible for the variability.

In our coupled model, the magnitude of the mean wind-stress forcing is determined from the vertical average of the meridional eddy momentum fluxes divergence in the atmosphere. An additional experiment has thus been performed to assess the influence of the amplitude of these fluxes (or equivalently of the wind-stress forcing) on the variability. The amplitude is modified through the dimensionless vertical profile of meridional eddy momentum fluxes that is specified as a function of height that resembles to observations (Vallis, 1982). This specification is justified since the vertical structure of the meridional eddy
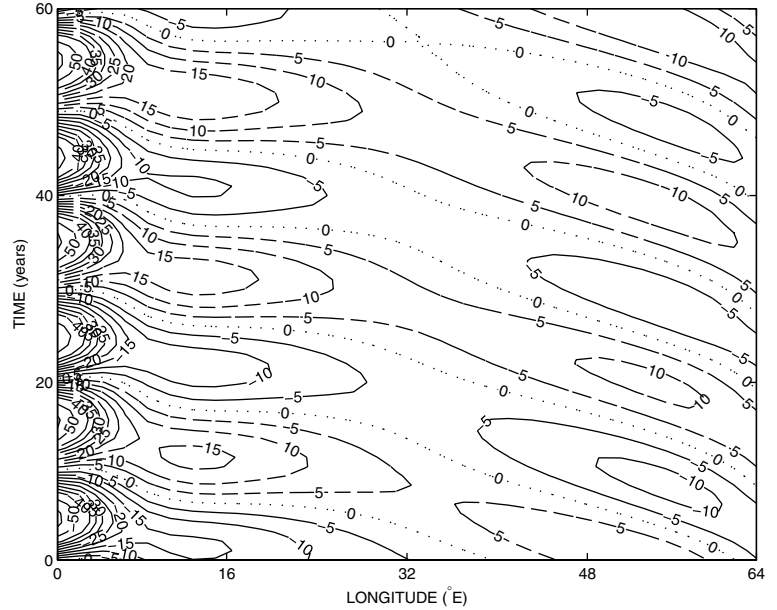
Fig. 8. Characteristic x-t diagram of density anomalies (10^{-3} kg m^{-3}) at 45°N at 325 m depth in CTRL. Solid (dotted-dashed) contours indicate positive (negative) values.

Table 3. Density variance budget (eq. 1) in the control experiment CTRL, basinwide averaged (angle brackets) and time averaged over one oscillation period (overbar). The driving term results from the interaction of eddy density flux with the mean density gradient: the contribution of temperature is dominant; salinity and crossing T/S terms are negligible (not shown). The contribution of surface buoyancy forcing is split into its thermal (*SHF*) and haline (*SSF*) components. The Heaviside step function $H(z)$ equals one in the forcing layer and is strictly zero elsewhere. The values are scaled with the absolute value of total dissipation which includes both convection and sub-grid scale mixing (last term of the rhs in eq. 1)

$\langle \frac{1}{2} \overline{\frac{\rho'^2}{\partial t}} \rangle$	-2×10^{-3}
$-\langle \overline{u' \rho'} . \nabla \overline{\rho} \rangle$	1.31
$-\alpha^2 \langle \overline{u' T'} . \nabla \overline{T} \rangle$	1.28
$\langle H(z) \overline{\rho' SHF'} \rangle$	-0.28
$\langle H(z) \overline{\rho' SSF'} \rangle$	-0.03
$\langle \overline{\rho' D'} \rangle$	1.00

momentum flux varies little with seasons and latitude, and has only little impact on the mean circulation (Stone and Yao, 1987). We found that increasing the magnitude of the meridional eddy momentum fluxes by 10% compared to CTRL damps the inter-decadal variability on a timescale of about 200 yr shorter than in CTRL. This confirms that the larger wind-stress forcing, the stronger the damping of the thermohaline oscillation (not shown) as noted by Huck et al. (2001): these authors showed in particular that it is the mean upward Ekman pumping in the subpolar gyre

that damps the interdecadal thermohaline variability through its effect on both the mean circulation and the temperature anomalies. To summarize, the interdecadal variability is somewhat insensitive to the wind-stress variability but is strongly affected by the amplitude of the mean wind-stress forcing.

4.4. Sensitivity of the variability to oceanic eddy diffusivities

The flux-type interdecadal oscillations have been found to be quite sensitive to vertical and horizontal eddy diffusivities by Huck et al. (2001) and te Raa and Dijkstra (2002) using stand-alone ocean models forced by constant surface fluxes. In order to determine if the relationships between the variability and the oceanic eddy diffusivities deduced by these authors are also valid in our coupled model, we present herein the sensitivity of the interdecadal variability to horizontal (K_h) and vertical (K_v) oceanic mixing rates in Tables 4 and 5 respectively.

The sensitivity of interdecadal oscillations to K_h is in qualitative agreement with the results of Huck (2001) and te Raa and Dijkstra (2002): increasing K_h lengthens the oscillation period and reduces its amplitude. The variability is sustained for $K_h = 700$ m^2 s^{-1}, and disappears for values larger than 1500 m^2 s^{-1}. The flux-type variability was shown to occur through a Hopf bifurcation when the horizontal eddy diffusivity is used a a control parameter (Huck et al., 2001; te Raa and Dijkstra, 2002).

By contrast, the sensitivity of the variability to K_v differs substantially from that obtained by Huck et al. (2001). These authors found that an increase in K_v strengthens the circulation and the oscillation amplitude and lengthens the period. In our coupled model, however, an increase in K_v from 0.3×10^{-4} m^2 s^{-1} to
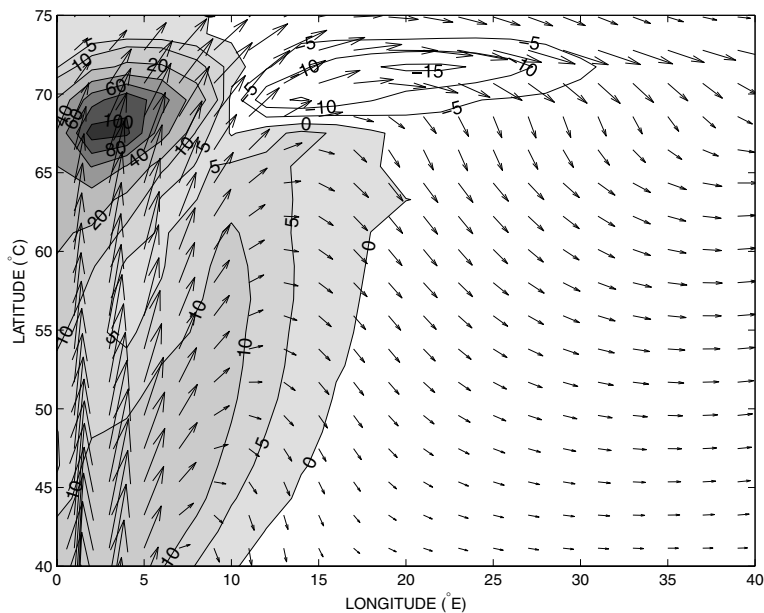
Fig. 9. The driving term of the equation for the density variance (eq. 1) averaged over one oscillation period and in the upper 250 m between 40 and 75 latitude in the Northern Hemisphere in CTRL $(-\overline{u'\rho'}.\nabla\overline{\rho}, \times 10^{-4}\ (\mathrm{kg\,m^{-3}})^2\ \mathrm{yr^{-1}})$. The mean surface circulation averaged in the upper 250 m is superimposed. Positive values (shaded) indicate a density variance growth.
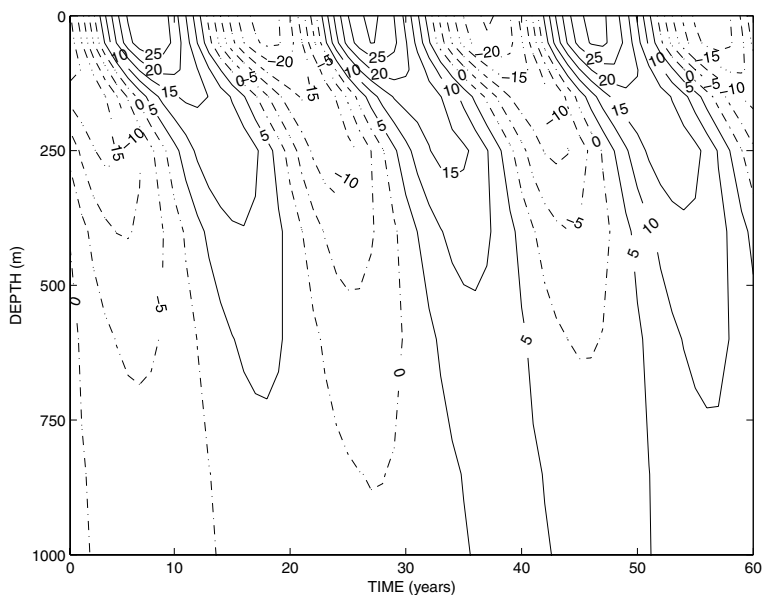

Fig. 10. Characteristic z-t diagram of density anomalies $(10^{-2}\ \mathrm{kg\,m^{-3}})$ during three oscillation cycles in CTRL. The perturbations are horizontally-averaged in an area of the unstable region defined as $[3–9°\mathrm{E}] \times [45–70°\mathrm{N}]$. The deep levels lag the upper anomalies by about one quarter period.

2×10^{-4} m^2 s^{-1} generally weakens the MOC, tends to reduce the oscillation period, and increases (decreases) the oscillation amplitude when K_v is smaller (larger) than 1.5×10^{-4} m^{2}s^{-1}. Furthermore, the smallest damping rates of interdecadal oscillations appear for intermediate values of K_v of roughly 10^{-4} m^2 s^{-1}. This contrasting behaviour between the uncoupled (forced) experiments carried out by Huck et al. (2001) and coupled experiments presented here suggests a potential influence of air–sea interactions in determining the sensitivity of the variability to K_v. A more complete analysis than the one presented here will be needed to determine the origin of this interesting behaviour, but is outside the scope of this paper.

5. Influence of a southern channel

Interdecadal variability has been mostly studied in the context of single hemisphere model geometries (Greatbatch and Zhang, 1995; Colin de Verdière and Huck, 1999; te Raa and Dijkstra, 2002, 2004; Kravtsov and Ghil, 2004). The oceanic thermohaline circulation in our two-hemisphere basin remains in a symmetric state, although it is known that multiple equilibria may exist and the symmetric circulation may shift spontaneously to a more stable single asymmetric cell. In order to study the variability for such an asymmetric mean overturning, we open a 'Drake Passage' that would certainly trigger such a transition. The

Table 4. Sensitivity of the interdecadal oscillations to horizontal eddy diffusivity (K_h). Given are the maximum strength of the mean meridional overturning circulation (MOC), its standard deviation, the period of the variability (if any), and the growth rate of oscillations computed using the timeseries of the mean kinetic energy density. The negative values indicate a damping of the oscillations. The three first quantities (MOC, std(MOC) and Period) are diagnosed over years 100–200 of the integrations which last 500 yr for each experiment. All experiments start from the same initial conditions, that are those used for CTRL

| K_h (m^2 s^{-1})	700	1000	1300	1500
MOC (Sv)	25.4	25.8	26.3	26.8
std(MOC) (Sv)	8.9	2.0	1.2	–
Period (yr)	20.0	20.0	25.0	–
Growth rate (yr^{-1})	−9456.0	−788.0	−62.3	–

Table 5. Same as Table 4 but for the sensitivity of the interdecadal oscillations to vertical eddy diffusivity (K_v)

K_v (10^{-4} m^2 s^{-1})	0.3	0.5	0.7	1.0	1.5	2.0
MOC (Sv)	33.3	30.8	28.7	25.8	22.6	22.9
std(MOC) (Sv)	–	–	0.5	2.1	2.7	2.0
Period (yr)	–	–	20.0	20.0	16.7	16.7
Growth rate (yr^{-1})	–	–	−142.0	−788.0	−176.3	−91.0

influence of the ACC on the interdecadal variability of the Atlantic thermohaline overturning has received little attention, although the ACC is known to have a large influence on the global circulation (e.g. Toggweiler and Samuels, 1995). In this section, we thus examine the effect of a periodic channel mimicking the ACC on the interdecadal variability in our coupled model. We apply periodic boundary conditions between 77°S and 60°S, but the ocean model remains flat-bottomed everywhere with a depth of 4500 m. As a consequence, no geostrophic meridional transport is allowed within this channel since no sill is considered. Coarse resolution ocean models such as the one used here overestimate the strength of the ACC because of the lack of mesoscale eddies and topographic ridges that increase the mean bottom drag. Thus, in order to simulate a zonal transport within the channel that agrees approximately with that observed, the horizontal Laplacian viscosity is enhanced from 10^5 to 6×10^5 m^2 s^{-1} everywhere. One final difference with the previous simulations carried out in geometries symmetric with respect to the equator is that we use a constant planetary albedo, the reason being that the annual mean atmospheric state becomes too asymmetric with respect to the equator with a Hadley cell in the SH about 10 times stronger than in the NH when the planetary albedo is temperature dependent. The asymmetry of the ITCZ shown here to be linked to the asymmetry of the ocean basin is certainly a desirable feature but the instability which appears is just too strong in this 2-D atmospheric model. The coupling procedure remains the same as before. The annual mean freshwater flux and wind-stress forcing diagnosed from the control atmosphere-only integration are applied to the ocean model with periodic boundary conditions in the SH, the SST being restored towards the same temperature profile as before. After this ocean spin-up, the coupled model is integrated for about 1000 yr.

The ocean mean state (Fig. 11) is obviously different from that simulated in CTRL. The meridional overturning circulation is now strongly asymmetric with respect to the equator, and exhibits a strong circulation cell (22 Sv) intensified in the NH and a reverse abyssal circulation (12 Sv) at depth in the SH. Deep
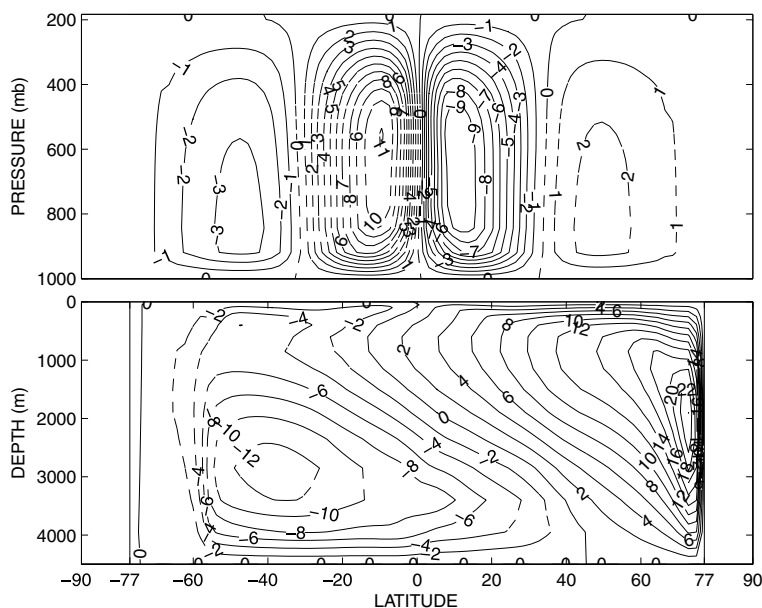
Fig. 11. Zonally-averaged circulation in the atmosphere (top panel, megaton s^{-1}) and in the ocean (bottom panel, Sv) averaged over one oscillation period (22 yr) of the ACC experiment which includes a southern channel between 77°S and 60°S. The flow is clockwise around solid contours.
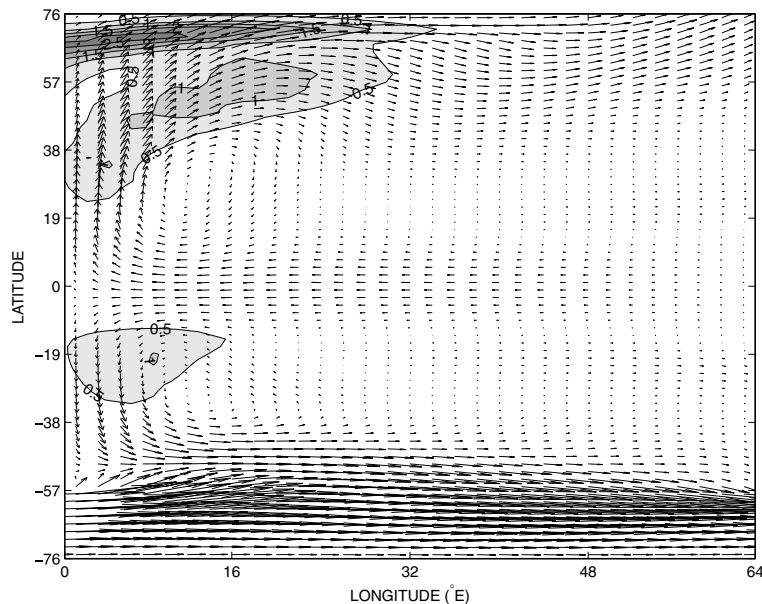
Fig. 12. Surface density variance (contours, $\times 10^3$ $(\mathrm{kg\ m^{-3}})^2$) averaged over one oscillation period of the ACC experiment. The mean surface current averaged in the upper 250 m is superimposed.

waters originating from the SH are now able to flow across the equator and reach 30°N in qualitative accordance with observations. The northward ocean heat transport reaches 0.7 PW at 35°N, 0.1 PW at the equator and −0.5 PW at 35°S. The atmospheric mean state (Fig. 11) is similar to that obtained in the control run, but the mean and transient circulations are now slightly more energetic in the SH than in the NH in agreement with the higher meridional temperature gradient in the atmosphere in the SH.

The coupled system generates spontaneous interdecadal oscillations with a period of 25 yr, close to that obtained in CTRL. However, a marked difference with CTRL is that the variability of the deep ocean circulation is now entirely confined to the NH, and is therefore strongly asymmetric with respect to the equator (Fig. 6d). In the SH, substantial variations of sea surface density are simulated (Fig. 12) and are dominated by changes in upward advection of salty waters associated with interdecadal variations of the large-scale overturning. The overall mechanism sustaining the variability in the NH remains exactly the same as before. In particular, changes in the overturning are not related to varying winds in the latitude band of the channel, as the variability persists under fixed surface flux (not shown). Huck et al. (2001) showed that the interdecadal variability obtained in box-ocean models forced by fixed surface fluxes is retained when east-west periodic boundary conditions are applied at all latitudes. They concluded that the decadal variability does not require boundary waves along the western and eastern boundaries. They attributed, however, the persistence of their oscillation to the large heat flux forcing employed (measured as the amplitude of the meridional distribution of surface heat flux) which induces, at equilibrium, a large vertical shear in the upper levels and is more likely to be baroclinically unstable than those associated with weaker surface

forcings. Here, the presence of the southern channel induces a relatively weak upper circulation in the SH that does not promote the baroclinic instability mechanism. As a consequence, no perturbations emerge in the SH and the variability is thus asymmetric with respect to the equator. Additional sensitivity experiments with narrower channels have been performed (not shown). The results are similar to those described here, with the interdecadal variability only apparent in the NH.

6. Summary and discussion

We have analysed interdecadal climate variability in a simplified coupled ocean–atmosphere model made of a 3-D flat-bottom planetary geostrophic ocean model and a 2-D ZACM atmospheric model. Our results show that the interdecadal variability found previously by many authors in different stand-alone ocean models forced by fixed surface fluxes (Greatbatch and Zhang, 1995; Colin de Verdière and Huck, 1999; Kravtsov and Ghil, 2004; te Raa and Dijkstra, 2002, 2004) is robust to additional freshwater feedbacks associated to the hydrological cycle simulated by the ZACM. In our coupled model, neither the surface flux variability nor the coupled air–sea feedbacks are indeed essential to the oscillation. In agreement with the flux-type nature of the variability, we show that the basic mechanism that lies at the heart of the existence of the oscillation is a regional baroclinic instability of the mean flow in the vicinity of the western boundary region. The spatial pattern of the variability is characterized by large and quasi-stationary temperature-dominated density anomalies in the northwestern quadrant of the ocean basin. In this region, the deep density anomalies lag the upper anomalies by about one quarter period. In the ocean interior, a westward propagation responsible for the adjustment of the

oscillation is clearly visible at mid-latitudes at depth. When an east-west periodic channel mimicking the Antarctic Circumpolar Current is present at high latitudes of the SH, both the mean overturning and the variability become asymmetric with respect to the equator and the interdecadal anomalies develop only in the NH with the same features as in the symmetric case. We suggest that the weakness of the upper ocean circulation in the SH which is not favourable to the baroclinic instability mechanism explains this interhemispheric difference.

The mechanism of spontaneous symmetry breaking (Quon and Ghil, 1992; Thual and McWilliams, 1992; Dijkstra and Molemaker, 1997) leading to asymmetric meridional overturning circulation states under symmetric forcing does not occur in our coupled model: the solution remains symmetric with respect to the equator in the case of the equatorially symmetric forcings and geometry (CTRL). One possible cause is that the freshwater forcing computed by the model is too low to permit transitions towards asymmetric states. The results presented here could be reexamined in the context of asymmetric thermohaline flows yet we feel confident that the basic mechanism of the interdecadal variability will remain identical to the one described in the present study as it persists in the experiment using an equatorially asymmetric geometry with an idealized ACC.

Since the salinity changes are not essential to the oscillatory behaviour found herein, our oscillation can be thus referred to as a thermally driven mode. This contrasts with the interdecadal variability simulated with AOGCMs in which the modifications of salinity in the sinking region of the North Atlantic play apparently a crucial role in modulating the North Atlantic Deep Water formation and ultimately the large-scale AMOC (Delworth et al., 1993; Timmermann et al., 1998; Delworth and Greatbatch, 2000; Dong and Sutton, 2005). The lack of a sea ice component in our model and the use of a linear equation of state for seawater are potential causes for this difference. Without sea ice effects, the interdecadal mode found by Yang and Neelin (1993, 1997) based on the interaction between sea ice melting/freezing and anomalous meridional heat transport associated with the AMOC cannot be reproduced. Kravtsov and Ghil (2004) have indeed considered a sea ice component, but in the framework of an ocean model without active salinity. The next step would be then to include a simple thermodynamic sea ice model with freshwater feedbacks.

Proxy climate indicators have revealed a multidecadal variability in the entire Atlantic basin with surface temperature anomalies of opposite signs between the NHs and SHs (Mann et al., 1998). In our simulation including an idealized ACC, the variability of surface air/sea temperature is weak in the SH and does not compare directly with these observations. The weakness of the variability of the poleward ocean heat transport in the SH combined with the eventually too large damping of SST anomalies by the atmosphere could explain this. On the other hand, the spatial pattern of SST anomalies shows encouraging similarities

with that obtained in the GFDL coupled model (Delworth et al., 1993) and that extracted from observational data (Levitus, 1989), with a SST dipole in the northwestern area of the North Atlantic (Fig. 7 vs Fig. 6(a) and (b) in Delworth et al., 1993). In addition, te Raa and Dijkstra (2004) noted that the relation between the sea surface temperature (density) anomalies in the northwestern corner of the basin and the meridional overturning is similar in their box-ocean model forced by constant surface fluxes and that of Delworth et al. (1993). These similarities suggest that the mode of variability of Delworth et al. (1993) could also be explained by a thermally driven mode obtained under constant surface fluxes, that is the same mode as the one identified here. Saravanan et al. (2000) also indicate that some uncertainties persist in the nature (flux or mixed type) of the interdecadal variability found in their idealized coupled model. Because the methodology proposed by Arzel et al. (2006) has been used successfully here to decipher the nature of the interdecadal oscillations in a coupled model, we suggest that it could be very useful in the aforementioned studies which use more realistic model components either with respect to geometry or resolved physics.

7. Acknowledgments

References

Arzel, O. 2004. Mécanismes de variabilité climatique interdécennale dans des modèles idealisés, Thèse de doctorat de l'Université de Bretagne Occidentale, 242 pages, Brest, France.

Arzel, O., Huck, T. and Colin de Verdière, A. 2006. The different nature of the interdecadal variability of the thermohaline circulation under mixed and flux boundary conditions. *J. Phys. Oceanogr.* **36**, 703–1718.

Branscome, L. E. 1983. A parameterization of transient eddy heat flux on a beta-plane. *J. Atmos. Sci.* **40**, 2508–2521.

Chen, F. and Ghil, M. 1995. Interdecadal variability of the thermohaline circulation and high-latitude surface fluxes. *J. Phys. Oceanogr.* **25**, 2547–2568.

Chen, F. and Ghil, M. 1996. Interdecadal variability in a hybrid coupled ocean-atmosphere model. *J. Phys. Oceanogr.* **26**, 1561–1578.

Colin de Verdière, A. 1988. Buoyancy driven planetary flows. *J. Mar. Res.* **46**, 215–265.

Colin de Verdière, A. and Huck, T. 1999. Baroclinic instability: an oceanic wavemaker for interdecadal variability. *J. Phys. Oceanogr.* **29**, 893–910.

Delworth, T. L. and Greatbatch, R. J. 2000. Multidecadal thermohaline circulation variability excited by atmospheric surface flux forcing. *J. Clim.* **13**, 1481–1495.

Delworth, T. L. and Mann, M. E. 2000. Observed and simulated multi-decadal variability in the northern hemisphere. *Clim. Dyn.* **16**, 661–676.

Delworth, T. L., Manabe, S. and Stouffer, R. J. 1993. Interdecadal variations of the thermohaline circulation in a coupled ocean-atmosphere model. *J. Clim.* **6**, 1993–2011.

Deser, C. and Blackmon, M. L. 1993. Surface climate variations over the north Atlantic during winter: 1900–1989. *J. Clim.* **6**, 1743–1753.

Dijkstra, H. A. and Molemaker, M. J. 1997. Symmetry breaking and overturning oscillations in thermohaline-driven flows. *J. Fluid. Mech.* **331**, 169–198.

Dong, B. and Sutton, R. T. 2005. Mechanism of interdecadal thermohaline circulation variability in a coupled ocean-atmosphere GCM. *J. Clim.* **18**, 1117–1135.

Genthon, C., Le Treut, H., Jouzel, J. and Sadourny, R. 1990. Parametrization of eddy sensible heat transports in a zonally averaged dynamic model of the atmosphere. *J. Atmos. Sci.* **47**, 2475–2487.

Gray, S. T., Graumlich, L. J., Betancourt, J. L. and Pederson, G. T. 2004. A tree-ring based reconstruction of the Atlantic Multidecadal Oscillation since 1567 AD. *Geophys. Res. Lett.* **31**, doi:10.1029/2004GL019932

Green, J. S. A., 1970. Transfer properties of the large-scale eddies and the general circulation of the atmosphere. *Quart. J. Roy. Meteorol. Soc.* **96**, 157–185.

Greatbatch, R. J. and Zhang, S. 1995. An interdecadal oscillation in an idealized ocean basin forced by constant heat flux. *J. Clim.* **8**, 81–91.

Hakkinen, S. 2000. Decadal air-sea interaction in the North Atlantic based on observations and modeling results. *J. Clim.* **13**, 1195–1219.

Hansen, D. V. and Bezdek, H. F. 1996. On the nature of decadal anomalies in North Atlantic sea surface temperature. *J. Geophys. Res.* **101**, 8749–8758.

Hougthon, J. T. and co-authors, 2001. IPCC 2001: Climate Change 2001: The scientific basis, Contribution of Working Group 1 to the third assessment report of Intergovernmental Panel on Climate Change. Cambridge University Press, Cambridge, United Kingdom and New York, USA, 881 pp.

Huck, T., Colin de Verdière, A. and Weaver, A. 1999. Interdecadal variability of the thermohaline circulation in box-ocean models forced by fixed surface fluxes. *J. Phys. Oceanogr.* **29**, 865–892.

Huck, T., Vallis, G. and Colin de Verdière, A. 2001. On the robustness of the interdecadal modes of the thermohaline circulation. *J. Clim* **14**, 940–963.

Kravtsov, S. and Ghil, M. 2004. Interdecadal variability in a hybrid coupled ocean-atmosphere model. *J. Phys. Oceanogr.* **34**, 1756–1775.

Kushnir, Y. 1994. Interdecadal variations in north Atlantic sea surface temperature and associated atmospheric conditions. *J. Clim.* **7**, 141–157.

Ledwell, J. R., Watson, A. J. and Law, C. S. 1993. Evidence for slow mixing across the pycnocline from an open-ocean tracer-release experiment. *Nature* **364**, 701–703.

Levitus, S. 1989. Interpendatal variability of temperature and salinity of intermediate depths of the north Atlantic ocean, 1970–1974 versus 1955–1959. *J. Geophys. Res.* **94**, 6091–6131.

McCracken, M. C. and Ghan, S. J. 1988. Design and use of zonally averaged models. In: *Physically-Based Modeling and Simulation of Climate and Climate change, Part II* (ed. M. E. Schlesinger), Riedel, 755–809.

Manabe, S., Smagorinsky, J. and Strickler, R. F. 1965. Simulated climatology of a general circulation model with a hydrological cycle. *Monthly Weather Rev.* **93**, 769–798.

Mann, M. E., Bradley, R. S. and Hugues, M. K. 1998. Global-scale temperature patterns and climate forcing over the past six centuries. *Nature* **392**, 779–787.

Munk, W. 1996. Abyssal recipes. *Deep-Sea Res* **13**, 707–730.

Munk, W. and Wunsch, C. 1998. Abyssal recipes II: energetics of tidal and wind mixing. *Deep-Sea. Res.* **45**, 1977–2010.

Ollitrault, M. and Colin de Verdière, A. 2002. SOFAR floats reveal mid-latitude intermediate North Atlantic general circulation. Part II: an Eulerian Statistical View. *J. Phys. Oceanogr.* **32**, 2034–2053.

Peixoto, J. P. and Oort, A. H. 1992. *Physics of Climate.* American Institute of Physics, New York, 520pp.

Quon, C. and Ghil, M. 1992. Multiple equilibria in thermosolutal convection due to salt-flux boundary conditions. *J. Fluid. Mech.* **245**, 449–484.

Reverdin, G., Cayan, D. and Kushnir, Y. 1997. Decadal variability of hydrography in the upper northern north Atlantic in 1948–1990. *J. Geophys. Res.* **102**, 8505–8531.

Salmon, R. 1986. A simplified linear ocean circulation theory. *J. Mar. Res.* **44**, 695–711.

Saravanan, R. and McWilliams, J. C. 1995. Multiple equilibria, natural variability, and climate transitions in an idealized ocean-atmosphere model. *J. Clim.* **8**, 2296–2323.

Saravanan, R., Danabasolglu, G. and Doney, S. C., McWilliams, J. C. 2000. Decadal variability and predictability in the midlatitude ocean-atmosphere system. *J. Clim.* **13**, 1073–1097.

Schlesinger, M. E. and Ramankutty, N. 1994. An oscillation in the global climate system of period 65-70 years. *Nature* **367**, 723–726.

Stone, P. H. 1972. A simplified radiative-dynamical model for the static stability of rotating atmospheres. *J. Atmos. Sci.* **29**, 405–418.

Stone, P. H. and Yao, M. S. 1987. Development of two-dimensional zonally averaged statistical-dynamical model. Part II: the role of eddy momentum fluxes in the general circulation and their parameterization. *J. Atmos. Sci.* **44**, 3769–3786.

Stone, P. H. and Yao, M. S. 1990. Development of two-dimensional zonally averaged statistical-dynamical model. Part III: the parametrization of the eddy fluxes of heat and moisture. *J. Clim.* **3**, 726–740.

te Raa, L. A. and Dijkstra, H. A. 2002. Instability of the thermohaline circulation on interdecadal timescales. *J. Phys. Oceanogr.* **32**, 138–160.

te Raa, L. A., Gerrits, J. and Dijkstra, H. A. 2004. Identification of the mechanism of interdecadal variability in the North Atlantic Ocean. *J. Phys. Oceanogr.* **34**, 2792–2807.

Thual, O. and McWilliams, J. C. 1992. The catastrophe structure of thermohaline convection in a two-dimensional fluid model and a comparison with low-order box models. *Geophys. Astrophys. Fluid. Dyn.* **64**, 67–95.

Timmermann, A. and Latif, M. 1998. Northern hemispheric interdecadal variability: a coupled air-sea mode. *J. Clim.* **11**, 1906–1931.

Toggweiler, J. R. and Samuels, B. 1995. Effect of Drake Passage on the global thermohaline circulation. *Deep-Sea Res.* **42**, 477–500.

Trenberth, K. E. and Caron, J. M. 2001. Estimates of meridional atmosphere and ocean heat transports. *J. Clim.* **14**, 3433–3443.

Vallis, G. K. 1982. A statistical-dynamical climate model with a simple hydrological cycle. *Tellus* **34**, 211–227.

Vellinga, M. and Wu, P. 2004. Low-latitude freshwater influence on centennial variability of the Atlantic thermohaline circulation. *J. Clim.* **17**, 4498–4511.

Weaver, A. J. and Sarachik, E. S. 1991a. The role of mixed boundary conditions in numerical models of the ocean's climate. *J. Phys. Oceanogr.* **21**, 1470–1493.

Weaver, A. J. and Sarachik, E. S. 1991b. Evidence for decadal variability in an ocean general circulation model: an advective mechanism. *Atmos. Ocean* **29**, 197–231.

Weaver, A. J. and Valcke, S. 1998. On the variability of the thermohaline circulation in the GFDL coupled model. *J. Clim.* **11**, 759–767.

Weaver, A. J., Sarachik, E. S. and Marotzke, J. 1991. Freshwater flux forcing of decadal and interdecadal oceanic variability. *Nature* **353**, 836–838.

Weaver, A. J., Marotzke, J., Cummins, P. F. and Sarachik, E. S. 1993.

Stability and variability of the thermohaline circulation. *J. Phys. Oceanogr.* **23**, 39–60.

Winton, M. 1997. The damping effect of bottom topography on internal decadal-scale oscillations of the thermohaline circulation. *J. Phys. Oceanogr.* **27**, 203–208.

Winton, M. and Sarachik, E. S. 1993. Thermohaline oscillations induced by strong steady salinity forcing of ocean general circulation models. *J. Phys. Oceanogr.* **23**, 1713–1724.

Yang, J. and Neelin, J. D. 1993. Sea-ice interaction with the thermohaline circulation. *Geophys. Res. Lett.* **20**, 217–220.

Yang, J. and Neelin, J. D. 1997. Decadal variability in coupled sea-ice thermohaline circulation systems. *J. Clim.* **10**, 3059–3076.

Yao, M. S. and Stone, P. H. 1987. Development of a two-dimensional zonally averaged statistical-dynamical model. Part I: the parametrization of moist convection and its role in the general circulation. *J. Atmos. Sci.* **44**, 65–82.